



## Degree of Al-Si order in K-feldspar and its effect on K-feldspar's dissolution

Shanke Liu<sup>1,2,3,\*</sup> and Yuanyuan Zhai<sup>1,2,3,4</sup>

<sup>1</sup> Key Laboratory of Mineral Resources, Institute of Geology and Geophysics, Chinese Academy of Sciences, Beijing 100029, China

<sup>2</sup> Innovation Academy for Earth Science, Chinese Academy of Sciences, Beijing 100029, China

<sup>3</sup> College of Earth Sciences, University of Chinese Academy of Sciences, Beijing 100049, China

<sup>4</sup> Current address: Shenzhen Xinhua Middle School, Shenzhen 518109, China

### ARTICLE INFO

Submitted: May 2021

Accepted: October 2021

Available on line: July 2021

\* Corresponding author:  
liushanke@mail.iggcas.ac.cn

Doi: 10.13133/2239-1002/17479

How to cite this article:  
Liu S. and Zhai Y. (2021)  
Period. Mineral. 90, 359-369

### ABSTRACT

Dissolution or alteration of feldspars is controlled by many factors such as the crystal structure (e.g., Al/Si ordering), temperature, pH, surface area, organic acids, chemical affinity, and precipitation of secondary minerals. The effects of Al/Si ordering (i.e., the degree of Al/Si order) on the percentage of feldspar dissolution (i.e., the extent of feldspar alteration) have not been studied. In this study, the degree of Al/Si order of different types of K-feldspars (eleven specimens including one sanidine sample, five orthoclase samples and five microcline samples) were investigated and determined by both X-ray powder diffraction (XRPD) and Fourier transform infrared spectra (FTIR) method. Further dissolution experiments of K-feldspar samples were operated under the hydrothermal condition for exploring the effects of Al/Si ordering on their dissolution. Data analysis shows that there is a good positive correlation between the degree of Al/Si order obtained from XRPD and that from FTIR. Furthermore, the degree of Al/Si order has no measurable effects on the percentage of K-feldspars dissolution. The conclusion is based on the macroscopic statistics data obtained from 0.5 g powder particles of the hydrothermal product, and it basically agrees with the study of the microscopic interfacial mechanism: the hydrothermal dissolution is not affected by the structural type of K-feldspar, i.e., the Al/Si ordering.

Keywords: K-feldspar; the degree of Al/Si order; XRPD; FTIR; dissolution.

### INTRODUCTION

The feldspar group, as one of the most common types of minerals in the earth's crust, occupies almost half volume of the earth's crust (Liu et al., 2019). The feldspar minerals are aluminosilicates whose general formula is  $AT_4O_8$ .  $A$  is divalent Ca or Ba, and monovalent Na or K, and  $T$  is Al, Si. Their structures are composed of  $AlO_4$  and  $SiO_4$  tetrahedra (corner-sharing) linked in an infinite three-dimensional network. One of the most common feldspars is K-feldspar ( $KAlSi_3O_8$ ), including sanidine (monoclinic), orthoclase (monoclinic), and

microcline (triclinic), and plagioclase ( $Na_yCa_{1-y}Al_{2-y}Si_{2+y}O_8$ ,  $0 < y < 1$ ), including albite, oligoclase, andesine, labradorite, bytownite and anorthite.

Feldspar alteration or dissolution (e.g., feldspar weathering and soil formation) is ubiquitous and important in fields, such as resources and environmental sciences (Ciceri et al., 2017; Liu et al., 2017b; Manning, 2018; Manning et al., 2017). It plays important roles in many aspects including surficial weathering and soil development, mass transfer in hydrothermal systems, geological carbon sequestration (Yuan et al., 2019).

Alteration of feldspars may promote CO<sub>2</sub> sequestration by consumption of H<sup>+</sup>, generation of HCO<sub>3</sub><sup>-</sup>, and pH buffering of formation water, and this will have a positive effect on reducing the CO<sub>2</sub> concentration in the atmosphere (Tutolo et al., 2015; Zhang et al., 2018). The weathering of potassium-rich feldspar can provide potassium (K) and other minor elements for plants and take an important role on the K cycle in the earth crust (Blake et al., 2008). Potassium-rich feldspar can be directly applied to the soil as a fertilizer or by artificial hydrothermal treatment, showing multi functions and positive effects on improving the soil quality (Liu et al., 2017b; Manning et al., 2017; Mohammed et al., 2014). The low-temperature dissolution of natural K-feldspars in mild aqueous environments is extremely slow, i.e., the mean lifetimes of a 1 mm crystal of K-feldspar in an exogenic cycle are 520000 years (Lasaga, 1984). The very slow dissolution rate of feldspar greatly hampers its potential application in resources and environmental fields. However, the process of chemical reaction is sharply shortened to a few hours or tens of hours for K-feldspar under extreme hydrothermal condition (Liu et al., 2015; Liu et al., 2017b). Therefore, the study of feldspar dissolution including both natural and extreme condition is very necessary.

Feldspar dissolution can be affected by many factors such as the crystal structure (e.g., Al/Si ordering), temperature, pH, surface area, organic acids, chemical affinity, and precipitation of secondary minerals (Skorina and Allanore, 2015; Yuan et al., 2019). It is the results of removing surface reactive sites through heterogeneous reactions and generating new reactive sites from interior bulk minerals, i.e., the surface renewal (Graham and Bouwer, 2012). During the process of surface renewal, the distribution of Al atoms, which is crucial for the dissolution kinetics of tectosilicate minerals, differs significantly between the bulk environment and on the surface and their energies are both closely related to T<sub>1</sub> occupation (PedeVilla et al., 2016). By combining theoretical model and experiment, several authors showed that the distribution of Al between the Al-rich (T<sub>1</sub>)-type and the Si-rich (T<sub>2</sub>)-type of sites, i.e., the degree of Al/Si order (*Z*), affected dissolution incongruence predominantly (Yang et al., 2014). However, feldspars dissolution under both natural and experimental extreme hydrothermal condition showed that they could experience a coupled interfacial dissolution reprecipitation (CIDR) process, and the chemical composition measurements proved that all elements were released congruently (i.e. stoichiometric) from the K-feldspar structure, similar to mineral replacement reactions mediated by aqueous fluids ubiquitous in natural environments (Hellmann et al., 2012; Hellmann et al., 2021; Zhai et al., 2021; Zhai

et al., 2020). Hydrothermal experiments and nanometer-scale observations showed the surface alteration layer of amorphous material formed in situ at the expense of the K-feldspar structure, and the interface demarcated a spatially coincident nm-sharp chemical and structural discontinuity between the parent K-feldspar and the amorphous phase. This incongruence of dissolution in Yang et al.'s report seems inconsistent with the CIDR mechanism (Yang et al., 2014), and the inconsistency is possibly related to different experimental conditions, because the incongruent dissolution is generally regarded as a transient phenomenon and is typically observed during the initial stage of feldspar dissolution (Hellmann, 1995; Lee et al., 2008). For a practical application, scientists or technicians commonly show concerns about which factors or processes will greatly affect the production in view of point of economy. In this situation, it is more important for studying the factors related to the extent of hydrothermal reaction rather than the reaction mechanism. For example, during the practical application of K-feldspar as the fertilizer, the factors of affecting the extent of hydrothermal reaction are a key role because these factors will increase or decrease the production cost. Therefore, the objectives of this study are providing experimental data and discussing the effects of different degrees of Al/Si order on K-feldspar's dissolution under extreme hydrothermal condition from a view point of application.

#### K-FELDSPAR STRUCTURE AND ITS DEGREE OF AL/SI ORDER

In all feldspars, the key structural units are four-membered rings of TO<sub>4</sub> tetrahedra, and these corner-shared similar rings form double crankshaft-like chains extending parallel to *a* (Figure 1). There are two types of TO<sub>4</sub> rings in a chain; one is normal to the *b* axis and the other is approximately normal to the *a* axis (Figure 1). In the four-membered rings of TO<sub>4</sub> tetrahedral, there are two symmetrically nonequivalent tetrahedral sites, labelled T<sub>1</sub> and T<sub>2</sub>. The adjacent crankshaft chains are mirror (for monoclinic feldspars) or pseudomirror (for triclinic feldspars) images of each other across (010) planes at 1/4 and 3/4 along the *b* cell edge (Figure 1B).

The structures, properties, and their compositions of feldspars have been systematically reviewed and compiled by several authors (Brown, 1983; Ribbe, 1983). In addition to chemical composition, feldspars are characterized by their state of "order" or "disorder". The state of order is a convenient way to express the Al-Si distribution of the feldspar (the degree of Al/Si order), and is usually described by a single parameter, *Z*, defined as the difference of the atom mole fractions of Al in the two tetrahedral sites (Thompson, 1969). In monoclinic feldspars (e.g., sanidine or orthoclase), the state of order

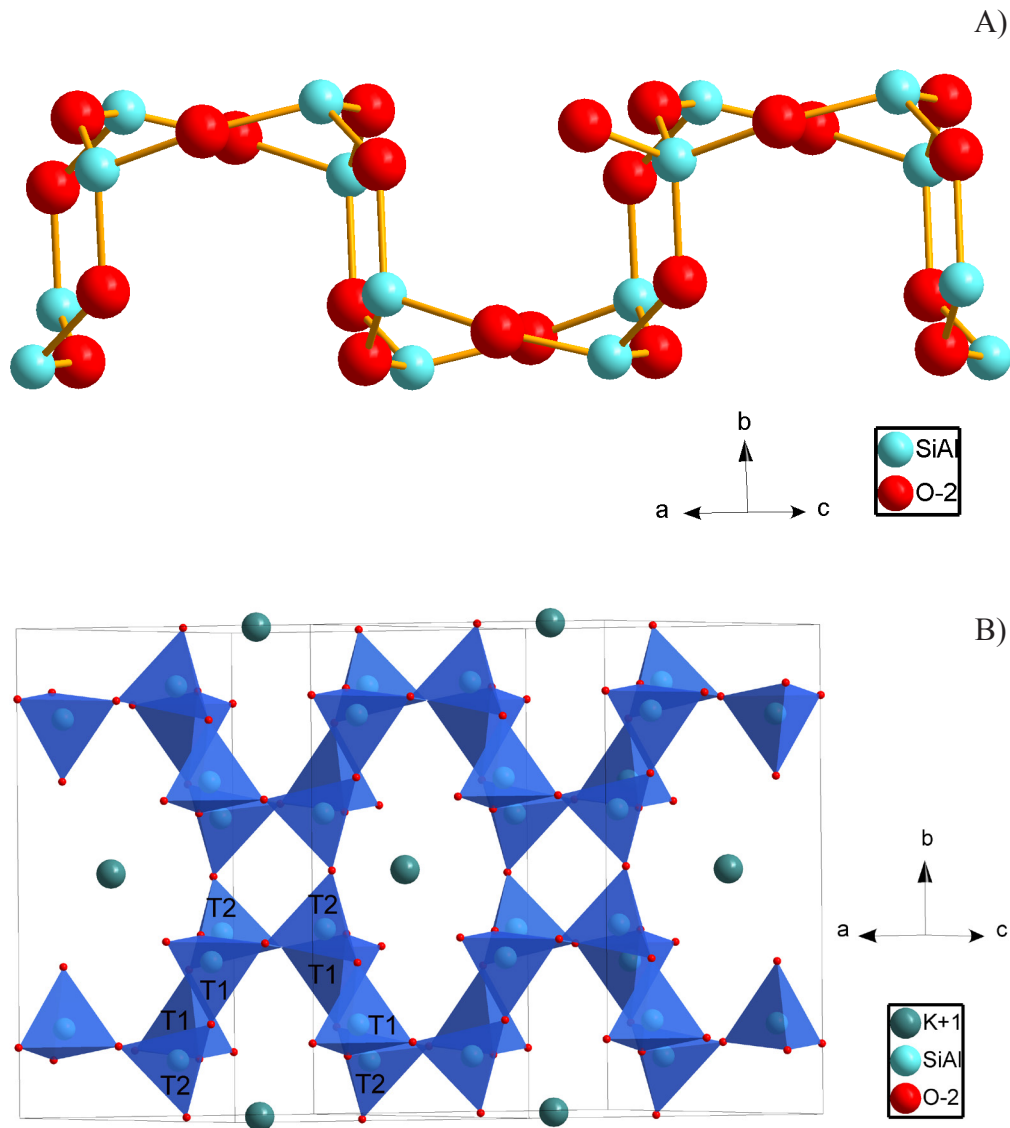


Figure 1. (A) left: the double crankshaft chain of four-membered tetrahedral rings that run parallel to  $a$  in all feldspars (only showing the outlined atoms). (B) right: a projection of double-crankshaft chains parallel to the  $a$  axis of K-feldspar with outlined  $\text{TO}_4$  tetrahedra.

is defined by the distribution of Al and Si between the two tetrahedral sites  $T_1$  and  $T_2$ , because the crystallographic symmetry between two  $T_1$  sites or between two  $T_2$  sites is equivalent. Therefore,

$$Z=2[t_1-t_2] \quad (1)$$

where  $t_1$  and  $t_2$  denote the Al contents of the  $T_1$  site and the  $T_2$  site, respectively ( $2t_1+2t_2=1$ ). In triclinic feldspar (such as microcline), the two T sites (two  $T_1$  or  $T_2$ ) are no longer symmetrically equivalent but are related by a pseudomirror parallel to the  $b$  axis. Therefore,  $o$  and  $m$  in triclinic feldspar are designated for differentiating two  $T_1$

or two  $T_2$  sites (Figure 2). Then, the degree of Al/Si order  $Z$  is expressed by the following equation:

$$Z=t_{1o}+t_{1m}-t_{2o}-t_{2m} \quad (2)$$

where  $t_{1o}$ ,  $t_{1m}$ ,  $t_{2o}$ , and  $t_{2m}$  denote the Al contents of the  $T_{1o}$ ,  $T_{1m}$ ,  $T_{2o}$ , and  $T_{2m}$  sites, respectively ( $t_{1o}+t_{1m}+t_{2o}+t_{2m}=1$ ).

## MATERIALS AND METHODS

### Samples

Eleven K-feldspar samples include one piece of sanidine, five pieces of orthoclase and five pieces of microcline. The sanidine sample (FHS-1) was picked

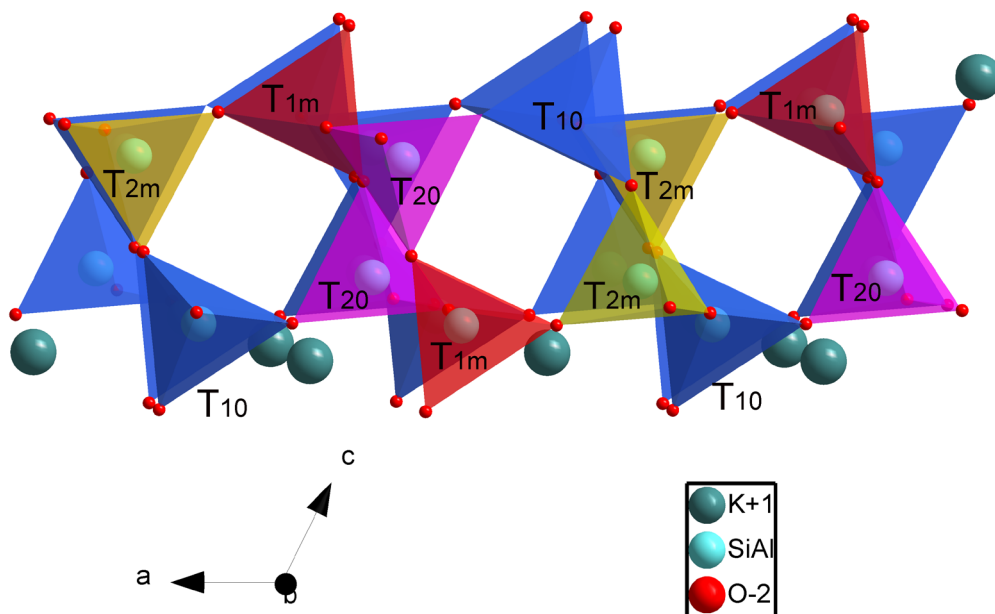


Figure 2. A portion of the triclinic K-feldspar structure showing the 4-membered tetrahedral rings.

up from the granite, near Hoh Xil region, Eastern Xinjiang Autonomous Region, China. Of five orthoclase samples (CHG-2, CHG-12, CSY-1, CSY-2, and CSY-3), CHG-2 and CHG-12 were from the granite-porphyr, near Songshan district, Chifeng city, Inner Mongolia Autonomous Region, China; CSY-1, CSY-2, and CSY-3 are from the orthophyre, in Xinghe county, Ulanqab City, Inner Mongolia Autonomous Region, China. Of five microcline samples (LS-1, LS-2, SX-1, TG-3, and TG-4), LS-1 and LS-2 were from the granite-pegmatite, in Lingshou county, Shijiazhuang city, Hebei province, China; SX-1 was from the orthophyre, in Song county, Luoyang City, Henan province, China; TYG-3 and TYG-4 were from the granite, in Balin Right Banner, Chifeng city, Inner Mongolia Autonomous Region, China. The details of these samples were described in the dissertation of Zhai (Zhai, 2020).

All the samples were dry crushed and ground in an agate mortar. K-feldspar grains were picked up by optical microscopy and heavy liquid separation, and then sieved, with the size fraction  $<74 \mu\text{m}$  being used for further treatments or analysis.

#### XRPD and degree of Al/Si order (Z) determination

All kinds of models of determining Al/Si distribution via X-ray method have been reviewed by Ribbe (Ribbe, 1983), Kroll and Ribbe (Kroll and Ribbe, 1987), and Jowhar (Jowhar, 2014). These models mainly base on a linear relation between the mean T-O bond length of a tetrahedron to its Al content. Methods of determining the

Al/Si distribution in alkali feldspars among nonequivalent tetrahedral sites are all model dependent, and different types of feldspars have been introduced into those models. An internal consistency possibly exists among those models, with  $\sum t_l = 2t_1$  or  $(t_{1o} + t_{1m})$  estimated to be about  $\pm 0.02$  and  $\Delta t_l = (t_{1o} - t_{1m})$  to be about  $\pm 0.03$  (Kroll and Ribbe, 1987).

Besides X-ray method, other methods are also explored and developed, such as Fourier transform infrared spectra (FTIR) (Harris et al., 1989; Lehtinen, 1974), Raman spectroscopy (Tribaudino et al., 2018), high resolution magic angle spinning multinuclear magnetic resonance spectroscopy (HR-MAS NMR) (Sanchez-Munoz et al., 2013), thermoluminescence (Polymeris et al., 2013), transmission electron microscopy (TEM) (Tafto and Buseck, 1983), channeling-enhanced microanalysis (ALCHEMI) based on TEM (Wu and Veblen, 2010).

Routine in-house X-ray power diffraction has difficulty in identifying different elements with similar scattering power, such as Al and Si in K-feldspar due to their same crystallographic site. However, the determination of Al/Si distribution in alkali feldspar using X-ray was achieved by indirect methods because there was a close relation between the degree of Al/Si order (Z) and lattice parameters (Kroll and Ribbe, 1987). For monoclinic alkali feldspars,

$$\sum t_1 = 2t_1 = \frac{b - 24.8095 + 74.9054c^*}{-3.3261 + 19.5012c^*} \quad (3)$$

For triclinic alkali feldspars,

$$\sum t_1 = t_1o + t_1m = \frac{b-21.5398+53.8405c^*}{2.1567-15.8583c^*} \quad (4)$$

$$\Delta t_1 = t_1o - t_1m = \frac{\gamma^*-44.778-0.50246\alpha^*}{6.646-0.05061\alpha^*} \quad (5)$$

where,  $b$ ,  $c^*$ ,  $\gamma^*$ , and  $\alpha^*$  are the parameters of feldspar's direct cell and reciprocal cell.

In this study, the authors applied above-stated Equations (3), (4), (5) and X-ray powder diffraction (XRPD) data to calculate the degree of Al occupancy in K-feldspar. XRPD patterns of K-feldspars were collected using a Panalytica X'Pert Pro diffractometer with  $CuK\alpha$  radiation at 40 kV and 40 mA, a 0.0167° step size over a 2 $\theta$  range of 10-90° at the Institute of Geology and Geophysics, Chinese Academy of Sciences (IGGCAS). XRPD data were fitted and refined by the Rietveld method using the computer program package GSAS (Larson and Von Dreele, 2004) and its graphical interface EXPGUI (Toby, 2001). The instrumental parameter file was obtained from the XRPD pattern of LaB<sub>6</sub> standard (SRM 660b, National Institute of Standards and Technology, USA). The starting atomic coordinates, cell parameters, equivalent isotropic displacement parameters, and space groups of sanidine, orchoclose, microcline, albite, quartz, and kaolinite were based on Gering (Gering, 1985), Colville and Ribbe (Colville and Ribbe, 1968), Dal Negro et al. (1978), Wenk and Kroll (Wenk and Kroll, 1984), d'Amour et al. (d'Amour et al., 1979), and Bish (Bish, 1993) respectively. The background was modeled with six-term shifted Chebyshev polynomial function. The peak-profile parameters were modelled using a modified TCH-pseudo-Voigt function modified by axial divergence (Finger et al., 1994) and as implemented in Profile function 3 in GSAS. Because of severe preferred orientation of powder feldspars, the spherical harmonics function and March-Dollase function were applied for describing them for K-feldspar and albite, respectively. Although K-feldspar grains were purified and picked up by the routine method, the XRPD analysis showed, apart from the major phase K-feldspar, all the samples except FHS-1 contained some impurities including albite, quartz, and kaolinite. Considering the resolution of XRPD data and quantities of atom parameters included in the Rietveld model, only cell parameters of all phases were optimized for avoiding a pseudo convergence.

#### Fourier transform infrared spectra (FTIR) analysis

The X-ray methods yield information of the unit-cell parameters, lattice symmetry and long-range order, however, the infrared absorption spectrum gives direct information about the immediate neighborhood of Si,

Al and alkali atoms in the feldspar structure. Therefore, FTIR as a routine technique to characterize local structure variations in feldspars has been applied and discussed by many authors (Atkinson et al., 1999; Harris et al., 1989; Lehtinen, 1974; Ma, 1988; Theodosoglou et al., 2010; Zhang et al., 1997; Zhou et al., 1997). In the spectra of alkali-feldspars, two most sensitive bands at around 540 and 640 cm<sup>-1</sup> respectively, were identified to be closely related to the Al/Si ordering and attributed to O-Si(Al)-O bend vibration (644 cm<sup>-1</sup>) and O-Si-O bend and K-O, Na-O stretching vibration (540 cm<sup>-1</sup>). Then, the degree of Al/Si order can be calculated using the following equations:

$$Z=0.05(\Delta\nu-90) \quad (6)$$

where,  $\Delta\nu$  is the wavenumber difference between FTIR band at around (644 cm<sup>-1</sup>) and FTIR band at around 540 cm<sup>-1</sup> for K-feldspar (Ma, 1988).

The samples were further ground with potassium bromide at a 1:10 ratio till the blends were homogeneously mixed. The mixture was then packed into the sample holder of the FTIR module. The spectra of K-feldspars were recorded with a rapid scan mode and 4000~400 cm<sup>-1</sup>, using a Bruker VERTEX 70v FT-IR spectrometer at room temperature. The resolution of the FTIR analysis was 4 cm<sup>-1</sup>, and the peak positions were identified using the OMNIC program.

#### Dissolution experiment

The dissolution experiment was explicitly reported in the dissertation of Zhai (Zhai, 2020), and only a brief narration was summarized here. Eleven K-feldspar samples were reacted through batch experiment. For each experiment, 1 g of K-feldspar grains was mixed with 1 g of fresh CaO reagent, and then 10 ml of deionized water were added. The admixture was stirred for 5 minutes before being sealed in a 100 mL stainless steel autoclave. The autoclave was put into an oven (pre-heated to 190 °C) and kept for 24 h at 190 °C. The autoclave was then cooled down to room temperature, and the hydrothermal materials in the autoclave were heated to 105 °C for 12 h for vaporizing remaining water. The retrieved solid cake was then reground by mortar and pestle to a size fraction <74 μm (hereafter 'hydrothermal product') for further analyses.

For quantifying the dissolution, i.e., the dissolution percentage, each 0.5 g hydrothermal product was added to 50 mL of 0.5 mol/L HCl solution, and then shaken over one hour at room temperature. A 2 mL filtrate was extracted from each mixture and then diluted with 48 mL of pure water. For all experiments, the resultant solutions were analyzed to determine the concentrations of K by inductively coupled plasma-optical emission spectroscopy (ICP-OES) using matrix-matched standards. The limit of

detection was  $3\sigma$  ( $\sigma$  is the standard deviation of blank determination), and the relative standard deviation was approximately 2.0%.

The percentage of K-feldspar dissolution ( $D$ , %) was approximately calculated from the following equation:

$$D\% = \frac{D_K}{M_K} \times 100 \quad (7)$$

where,  $D_K$  is the K element content of 0.5 g hydrothermal product dissolved in  $0.5 \text{ mol}\cdot\text{L}^{-1}$  HCl acid, and it can be obtained from the ICP-OES data, and  $M_K$  is the total K content of the corresponding 0.5 g hydrothermal product.  $M_K$  can be approximately equivalent to be the K content of 0.25g K-feldspar because of the small mass change before and after the hydrothermal reaction.

## RESULTS

The cell parameters of K-feldspars and quantitative phase analysis obtained by the Rietveld method were supplemented in Tables S1 and S2, respectively. Based on Equations (3), (4), (5), Al occupancy and  $Z$  were calculated (Table 1). The FTIR spectra at the wavenumber of 500-700  $\text{cm}^{-1}$  were plotted in Figure 3 and  $Z$  calculated from Equation (6) was listed in Table 2.  $Z$  values from FTIR

are greater than those from XRPD (Table 1). Considering the uncertainty introduced by calculation models and instruments, the errors of  $Z$  values from XRPD and FTIR were approximately equal to be about  $\pm 0.05$  and  $\pm 0.2$ , respectively. When  $Z$  obtained from FTIR are plotted against those from XRPD, the relationship shows a good correlation between them (Figure 4, Pearson's  $R=0.95$ ,  $P<<0.01$ ).

The dissolution percentage of K element in the K-feldspars were listed in Table 2, and the relative error of  $D$  (%) introduced by the ICP-OES measurement was about 6% ( $3\sigma$ ) in terms of Equation (7). The 56~70% dissolution percentage shows that the tetrahedra structure of K-feldspar is not subject to be decomposed and destroyed under the hydrothermal condition of this study. The details of the dissolution experiment, dissolution mechanism and phase analysis of eleven K-feldspar samples have been published in other journals (Hellmann et al., 2021; Zhai et al., 2020). In order to investigate the effect of Al/Si ordering on the dissolution percentage, the authors plotted the dissolution percentage against the degree of Al/Si order from XRPD (Pearson's  $R=0.41$ ,  $P=0.21$ ) and FTIR (Pearson's  $R=0.40$ ,  $P=0.22$ ), respectively, in Figure 5. Although  $Z$  from FTIR have larger errors than those from XRPD, they show a close correlation against the dissolution percentage of

Table 1. the degree of Al/Si order ( $Z$ ) calculated from XRPD and FTIR data.

Sample	Z from XRPD				Z from FTIR				
	Al occupancy		Z	Wavenumber ( $\text{cm}^{-1}$ )		Z			
	$2t_1$	$2t_2$		$\nu_1$	$\nu_2$				
Sanadine	FHS-1	0.61	0.39	0.22±0.05	638.26	540.93	0.37±0.2		
	Orthoclase	CHG-2	0.82	0.18	0.63±0.05	645.30	538.54	0.84±0.2	
		CHG-12	0.76	0.24	0.52±0.05	642.93	539.93	0.65±0.2	
	CSY-1	0.77	0.23	0.55±0.05	644.99	542.19	0.64±0.2		
	CSY-2	0.76	0.24	0.51±0.05	642.53	538.09	0.72±0.2		
	CSY-3	0.82	0.18	0.64±0.05	644.67	539.24	0.77±0.2		
		$t_{10}$	$t_{1m}$	$t_{20}$	$t_{2m}$				
Microcline	LS-1	0.72	0.24	0.02	0.02	0.92±0.05	647.01	538.63	0.92±0.2
	LS-2	0.77	0.13	0.05	0.05	0.79±0.05	646.82	538.61	0.91±0.2
	SX-1	0.66	0.27	0.03	0.03	0.86±0.05	646.33	538.43	0.90±0.2
	TG-3	0.48	0.35	0.08	0.08	0.67±0.05	645.27	540.09	0.76±0.2
	TG-4	0.48	0.36	0.08	0.08	0.68±0.05	644.49	539.79	0.74±0.2

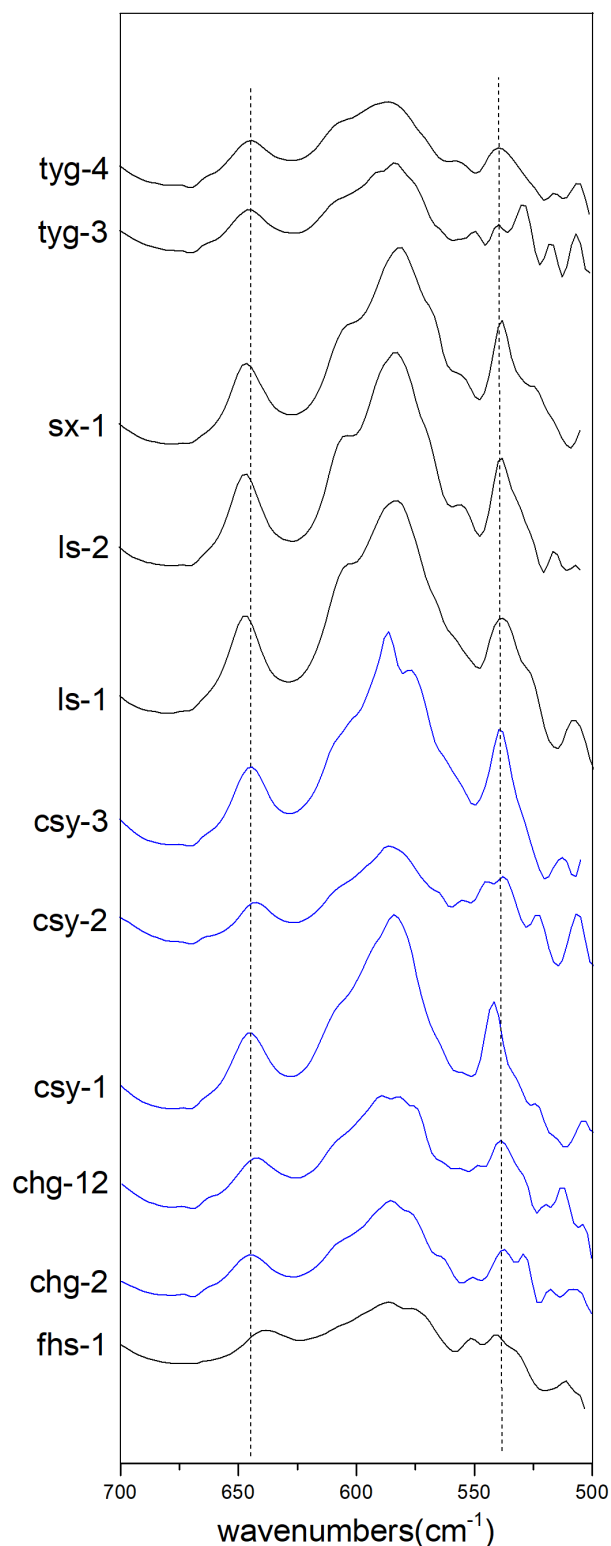


Figure 3. One region of Fourier transform infrared spectra of K-feldspar specimens ( $500\text{--}700\text{ cm}^{-1}$ ). Two dot lines are showed around two bands closely correlated with Al/Si ordering of K-feldspars.

K-feldspar. However, based on the criterion presented by Koo and Li (Koo and Li, 2016), the correlation is poor because of the small  $R$  factor ( $R < 0.5$ ).

## DISCUSSION

### The degree of Al/Si order ( $Z$ )

Even the high-resolution synchrotron X-ray diffraction had the difficulty in refining the Al occupancy in tetrahedral and had to undirectedly calculate it by T-O bond length (Yang et al., 2014). For routine X-ray powder diffraction, the data quality can guarantee the reliability of refining alkali feldspar structures (Liu et al., 2017a; Liu, 2015). Considering the existence of impurities such albite or quartz, the authors gave up refining the atom positions of K-feldspar. The robust refinement mode would not affect the precision of the results and the comparison of Al/Si ordering, as Angel and Nestola stated that “if different crystal structures of the same type (e.g., albites) are refined with exactly the same model, then X-ray structure refinement can yield precise values for the differences between the structures, and thus changes in the state of Al, Si order, even if the absolute values of site occupancies are less well-defined” (Angel and Nestola, 2016).

In a completely disordered sanidine (high sanidine,  $C2/m$ ), the Al, Si distribution is random, and  $Z$  is equivalent to 0 (i.e.,  $t_1=t_2=0.25$  or  $2t_1=2t_2=0.5$ ,  $Z=0$ ). When a sanidine crystal is cooled slowly from high temperature, Al migrates preferentially into the  $T_1$  sites and Si into the  $T_2$  sites in order to satisfy local electrostatic charge balance (the oxygens coordinating  $T_1$  are more closely bonded to the large  $K^+$  cation than those surrounding  $T_2$ ). In this study, the Al occupancy in  $T_1$  site (0.61) is larger than  $T_2$  site (0.39). Based on the definition of the boundaries for the terms *high* and *low sanidine* (HS, LS) and *orthoclase* (OR) (HS:  $0.5 < 2t_1 < 0.666$ ; LS:  $0.666 < 2t_1 < 0.74$ ; OR:  $0.74 < 2t_1 < 1.0$ ) (Brown, 1983), FHS-1 belongs to high sanidine.

If Al concentrates in one of  $T_1$  is larger than another, i.e.,  $t_{1o} > t_{1m}$ , these sites are no longer equivalent and the symmetry of K-feldspar is change into  $C\bar{1}$  (microcline). For maximum microcline, it is completely ordered (i.e.,  $t_{1o}=1.0$ ;  $t_{1m}=t_{2o}=t_{2m}=0$ ;  $Z=1$ ); for intermediate microcline, the degree of Al/Si order agrees with the following rules:  $t_{1o} > t_{1m} > t_{2o} \cong t_{2m}$ . The degree of Al/Si order of all five microcline are intermediate (Table 1).

Variations in the FTIR spectra provided insights into the effects of Al/Si ordering on structural properties, especially in the region of  $500\text{--}700\text{ cm}^{-1}$  (Figure 3). As above-stated, the most sensitive bands of wavenumbers closely related to the Al/Si ordering are at around  $540$  and  $640\text{ cm}^{-1}$  respectively. These bands were identified to be related to O-Si(Al)-O bend vibration ( $644\text{ cm}^{-1}$ ) and O-Si-O bend and K-O, Na-O stretching vibration ( $540\text{ cm}^{-1}$ ). Except the two bands in the region of

Table 2. Dissolution percentage of K in K-feldspar ( $D$ , %) and K content determined from ICP-OES.

Sample		K content in K-feldspar (%)	K content determined by ICP-OES (ppm)	$D_K$ (mg)	$M_K$ (mg)	$D$ (%)
Sanadine	FHS-1	8.55	246.50	12.33	21.37	57.04±3.42
	Orthoclase	CHG-2	9.68	303.00	15.15	24.19
	CHG-12	9.49	274.25	13.71	23.72	56.84±3.41
	CSY-1	9.53	308.00	15.40	23.83	63.98±3.84
	CSY-2	11.03	316.75	15.84	27.58	56.60±3.40
	CSY-3	11.16	394.25	19.71	27.91	69.94±4.20
Microcline	LS-1	10.64	323.50	16.18	26.61	60.48±3.63
	LS-2	10.86	340.25	17.01	27.15	61.32±3.68
	SX-1	11.79	371.50	18.58	29.47	62.25±3.74
	TG-3	9.28	292.00	14.60	23.20	62.60±3.76
	TG-4	11.04	331.00	16.55	27.59	59.64±3.58

500-700  $\text{cm}^{-1}$ , a major peak at around 580  $\text{cm}^{-1}$ , which was attributed to O-Si(Al)-O bending vibration. Several peaks appeared in the region of 500-560  $\text{cm}^{-1}$ , and they were attributed to be O-Si-O bend and K-O, Na-O stretching vibration, possibly related to those impurity phases. The wavenumbers of the peaks at 540  $\text{cm}^{-1}$  and 650  $\text{cm}^{-1}$  shift systematically with the ordering state of a sample (Atkinson et al., 1999; Theodosoglou et al., 2010; Zhang et al., 1997). In this study, the average values are

540.93, 539.60, 539.11, and 638.26, 644.08, 645.98 in the order of sanidine, orthoclase, and microcline, respectively (Figure S1), in accord with above-mentioned peak shift.

Because the high content such as albite or Na element in samples (Table S2), the effects of both Na and albite content on Al/Si ordering were analyzed by plotting the degree of Al/Si against Na and albite content (Figures S2 and S3 in the supplementary materials). Figures S2 and S3 show a poor negative and positive correlation for Na mole ratio vs degree of Al/Si order from XRPD and albite content vs degree of Al/Si order from XRPD, respectively. This is different from those Ca-bearing feldspars, i.e., plagioclase, because the increase of Ca content will change the atom ratio between Al and Si for balancing electric neutrality.

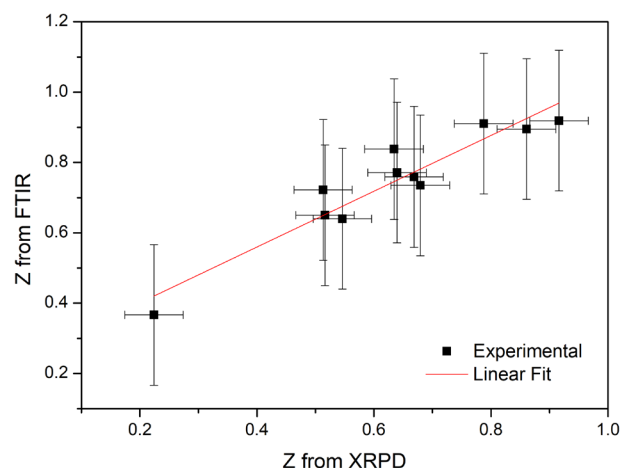


Figure 4. The degree of Al/Si order ( $Z$ ) obtained from FTIR data vs. XRPD data (Pearson's  $R=0.95$ ,  $P<<0.01$ ), and the  $Z$  from FTIR was beyond 1.0 for showing the error bar.

#### The effect of Al/Si ordering on dissolution of K-feldspar

Feldspar dissolution is a complicated process, and is affected by many factors (Skorina and Allamore, 2015; Yuan et al., 2019). However, recent studies showed that feldspar dissolution was a congruence coupled-interfacial-dissolution-precipitation (CIDR) process (Hellmann et al., 2012; Zhai, 2020; Zhai et al., 2020), and the dissolution mechanism was not affected by the structural type of K-feldspar, i.e., the Al/Si ordering (Zhai, 2020). Yang et al. obtained the dissolution rate by introducing the Al/Si ordering parameters into the model and combining techniques such as HR-XRD and FTIR (Yang et al., 2014). They found that the distribution of Al between T1 and T2 sites affected feldspars' dissolution

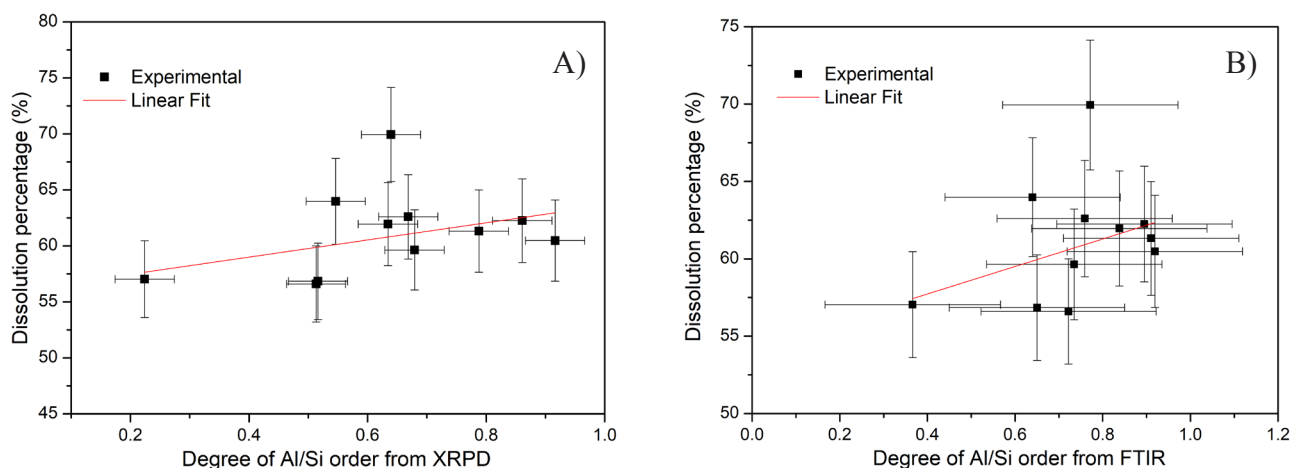


Figure 5. The K element dissolution percentage ( $D$  %) vs the degree of Al/Si order ( $Z$ ): (A, left) obtained from XRPD data for all K-feldspar samples (Pearson's  $R=0.41$ ,  $P=0.21$ ); (B, right) obtained from FTIR data for all K-feldspar samples (Pearson's  $R=0.40$ ,  $P=0.22$ ), and the range of horizontal axis was beyond 1.0 for showing the error bar.

incongruence predominantly. Their results appear inconsistent with CIDR mechanism reported by several authors (Hellmann et al., 2012; Zhai, 2020; Zhai et al., 2020). The inconsistency may be caused by the different experimental conditions, because the incongruent dissolution is in general a transient phenomenon and is typically observed during the initial stage of feldspar dissolution. However, these above-mentioned authors aimed at investigating the hydrothermal mechanism of feldspar and the reaction interface between feldspar and fluid, i.e., the mechanism that controlled how a primary K-feldspar mineral was structurally and chemically decomposed during the hydrothermal reaction, and they did not show how the extent of hydrothermal reaction was, i.e., how the percentage of K-feldspar dissolution is.

In this study, the evaluation of the dissolution experiment in terms of the percentage of K-feldspar dissolution ( $D$ , %) is a macroscopic statistical data obtained from 0.5 g powder particles of the hydrothermal product. This is different from the above-mentioned studies that focused on the reaction interface of feldspars. Although the dissolution percentage of K in K-feldspars appears to have a slightly positive correlation with the degree of Al/Si order, the relationship is very poor based on their correlation coefficient. Considering the magnitude of uncertainties associated with the data, the authors conclude that the degree of Al/Si order has no measurable effects on the percentage of K-feldspars dissolution.

## CONCLUSIONS

The degree of Al/Si order of different types of K-feldspars (eleven specimens including one sanidine sample, five orthoclase samples and five microcline samples) were

determined by both X-ray powder diffraction (XRPD) and Fourier transform infrared spectra (FTIR) method. The results of Al/Si ordering obtained from XRPD and FTIR show a good correlation (Pearson's  $R=0.94$ ,  $P\ll 0.01$ ). Through dissolution experiments of K-feldspars and comparison analysis, the dissolution of K-feldspars is not almost related to the degree of Al/Si order. The conclusion is based on the macroscopic average data obtained from 0.5 g powder particles of the hydrothermal product, and agree with the conclusion made from the microscopic interface study of K-feldspar hydrothermal reaction: the hydrothermal dissolution is not affected by the structural type of K-feldspar, i.e., the Al/Si ordering.

## Author contributions

SKL collected XRPD data and performed the calculations, YYZ carried out the dissolution and FTIR experiments.

## Declaration of competing interest

The authors declare that they have no known competing financial interests or personal relationships that could have appeared to influence the work reported in this paper.

## ACKNOWLEDGEMENTS

The study was supported by General projects of Beijing Natural Science Foundation (No. 8202048).

## REFERENCES

- Angel R. and Nestola F., 2016. A century of mineral structures: How well do we know them? *American Mineralogist* 101, 1036-1045.
- Atkinson A., Carpenter M., Salje E., 1999. Hard mode infrared

- spectroscopy of plagioclase feldspars. *European Journal of Mineralogy* 11, 7-21.
- Bish D., 1993. Rietveld refinement of the kaolinite structure at 1.5 K. *Clays and Clay Minerals* 41, 738-744.
- Blake G., Steinhart G., Pombal X., Muñoz J., Cortizas A., Arnold R., Schaetzl R., Stagnitti F., Parlange J., Steenhuis T., Chesworth W., Mualem Y., Morel-Seytoux H., Spaargaren O., Chesworth W., Soon Y., Orlov D., Spaargaren O., Oertli J., Gliński J., Lipiec J., Stepniewski W., Spaargaren O., Spaargaren O., Chesworth W., 2008. Potassium cycle. In Chesworth W., Ed. *Encyclopedia of Soil Science*, 583-587. Springer Netherlands, Dordrecht.
- Brown W., 1983. Feldspars and feldspathoids: Structures, properties and occurrences. Springer Science & Business Media.
- Ciceri D., de Oliveira M., Allanore A., 2017. Potassium fertilizer via hydrothermal alteration of K-feldspar ore. *Green Chemistry* 19, 5187-5202.
- Colville A. and Ribbe P., 1968. The crystal structure of an adularia and a refinement of the structure of orthoclase. *American Mineralogist* 53, 25-37.
- d'Amour H., Denner W., Schulz H., 1979. Structure determination of  $\alpha$ -quartz up to 68x108 Pa. *Acta Crystallographica Section B: Structural Crystallography and Crystal Chemistry* 35, 550-555.
- Finger L., Cox D., Jephcoat A., 1994. A correction for powder diffraction peak asymmetry due to axial divergence. *Journal of Applied Crystallography* 27, 892-900.
- Gering E., 1985. Silizium/Aluminium-Ordnung und Kristallperfektion von Sanidinen. Kernforschungszentrum.
- Graham A., Bouwer E., 2012. Oxidative dissolution of pyrite surfaces by hexavalent chromium: Surface site saturation and surface renewal. *Geochimica et Cosmochimica Acta* 83, 379-396.
- Harris M., Salje E., Guttler B., Carpenter M., 1989. Structural states of natural potassium-feldspar - an infrared spectroscopic study. *Physics and Chemistry of Minerals* 16, 649-658.
- Hellmann R., 1995. The albite-water system: Part II. The time-evolution of the stoichiometry of dissolution as a function of pH at 100, 200, and 300 °C. *Geochimica et Cosmochimica Acta* 59, 1669-1697.
- Hellmann R., Wirth R., Daval D., Barnes J., Penisson J., Tisserand D., Epicier T., Florin B., Hervig R., 2012. Unifying natural and laboratory chemical weathering with interfacial dissolution-precipitation: A study based on the nanometer-scale chemistry of fluid-silicate interfaces. *Chemical Geology* 294, 203-216.
- Hellmann R., Zhai Y., Robin E., Findling N., Mayanna S., Wirth R., Schreiber A., Cabié M., Zeng Q., Liu S., Liu J., 2021. The hydrothermal alkaline alteration of potassium feldspar: A nanometer-scale investigation of the orthoclase interface. *Chemical Geology* 569, 120133.
- Jowhar T., 2014. Methods for estimation of structural state of alkali feldspars. In Babu B., Nagar A., Deep K., Pant M., Bansal J., Ray K., and Gupta U., Eds. *Proceedings of the second international conference on soft computing for problem solving*, 236, 1003-1013.
- Koo T. and Li M., 2016. A guideline of selecting and reporting intraclass correlation coefficients for reliability research. *Journal of Chiropractic Medicine* 15, 155-163.
- Kroll H. and Ribbe P., 1987. Determining (Al, Si) distribution and strain in alkali feldspars using lattice-parameters and diffraction-peak positions - a review. *American Mineralogist* 72, 491-506.
- Larson A. and Von Dreele R., 2004. General Structure Analysis System (GSAS). Los Alamos National Laboratory Report (LAUR 86-748), Los Alamos, New Mexico, 224 pp.
- Lasaga A., 1984. Chemical-kinetics of water-rock interactions. *Journal of Geophysical Research* 89(NB6), 4009-4025.
- Lee M., Hodson M., Brown D., MacKenzie M., Smith C., 2008. The composition and crystallinity of the near-surface regions of weathered alkali feldspars. *Geochimica et Cosmochimica Acta* 72, 4962-4975.
- Lehtinen M., 1974. Degree of Al/Si order in potassium feldspars: A combination of X-ray and infrared data. *Contributions to Mineralogy and Petrology* 47, 223-230.
- Liu S., Li J., Liu J., 2017a. An updated model of Rietveld structure refinement of Na/K-feldspar. *Periodico di Mineralogia* 86, 75-85.
- Liu S., 2015. Rietveld structure refinement of microcline. *European Journal of Mineralogy* 27, 501-510.
- Liu S., Han C., Liu J., 2019. Study of K-feldspar and lime hydrothermal reaction: phase and mechanism with reaction temperature and increasing Ca/Si ratio. *Minerals* 9, 46.
- Liu S., Han C., Liu J., Li H., 2015. Hydrothermal decomposition of potassium feldspar under alkaline conditions. *RSC Advances* 5, 93301-93309.
- Liu S., Qi X., Han C., Liu J., Sheng X., Li H., Luo A., Li J., 2017b. Novel nano-submicron mineral-based soil conditioner for sustainable agricultural development. *Journal of Cleaner Production* 149, 896-903.
- Ma H., 1988. Comparison of K-feldspar ordering by X-ray powder and infrared spectroscopy and its relations to Al occupancy and equilibrium temperature. *Acta Mineralogica Sinica*, 143-150.
- Manning D., 2018. Innovation in resourcing geological materials as crop nutrients. *Natural Resources Research* 27, 217-227.
- Manning D., Baptista J., Limon M., Brandt K., 2017. Testing the ability of plants to access potassium from framework silicate minerals. *Science of the Total Environment* 574, 476-481.
- Mohammed S., Brandt K., Gray N., White M., Manning D., 2014. Comparison of silicate minerals as sources of potassium for plant nutrition in sandy soil. *European Journal of Soil Science* 65, 653-662.
- Pedevilla P., Cox S., Slater B., Chaelides A., 2016. Can ice-like structures form on non-ice-like substrates? the example of the

- K-feldspar microcline. *Journal of Physical Chemistry C* 120, 6704-6713.
- Polymeris G., Theodosoglou E., Kitis G., Tsirliganis N., Koroneos A., Paraskevopoulos K., 2013. Preliminary results on structural state characterization of K-feldspars by using thermoluminescence. *Mediterranean Archaeology and Archaeometry* 13, 15.
- Ribbe P., 1983. *Feldspar Mineralogy*. De Gruyter.
- Sanchez-Munoz L., Sanz J., Sobrados I., Gan Z., 2013. Medium-range order in disordered K-feldspars by multinuclear NMR. *American Mineralogist* 98, 2115-2131.
- Skorina T. and Allanore A., 2015. Aqueous alteration of potassium-bearing aluminosilicate minerals: from mechanism to processing. *Green Chemistry* 17, 2123-2136.
- Tafto J. and Buseck P., 1983. Quantitative study of Al-Si ordering in an orthoclase feldspar using an analytical transmission electron-microscope. *American Mineralogist* 68, 944-950.
- Theodosoglou E., Koroneos A., Soldatos T., Zorba T., Paraskevopoulos K., 2010. Comparative Fourier transform infrared and X-ray powder diffraction analysis of naturally occurred K-feldspars. *Bulletin of the Geological Society of Greece* 43, 2752-2761.
- Thompson J., 1969. Chemical reactions in crystals. *American Mineralogist* 54, 341-375.
- Toby B., 2001. EXPGUI, a graphical user interface for GSAS. *Journal of Applied Crystallography* 34, 210-213.
- Tribaudino M., Gatta G., Aliatis I., Bersani D., Lottici P., 2018. Al-Si ordering in albite: A combined single-crystal X-ray diffraction and Raman spectroscopy study. *Journal of Raman Spectroscopy* 49, 2028-2035.
- Tutolo B., Luhmann A., Kong X., Saar M., Seyfried W., 2015. CO<sub>2</sub> sequestration in feldspar-rich sandstone: Coupled evolution of fluid chemistry, mineral reaction rates, and hydrogeochemical properties. *Geochimica et Cosmochimica Acta* 160, 132-154.
- Wenk H. and Kroll H., 1984. Analysis of P-1, I-1 and C-1 plagioclase structures. *Bulletin de minéralogie* 107, 467-487.
- Wu J. and Veblen D., 2010. Characterization of Al-Si ordering state in an alkali feldspar using atom location by channeling-enhanced microanalysis (ALCHEMI). *American Mineralogist* 95, 41-46.
- Yang Y., Min Y., Lococo J., Jun Y., 2014. Effects of Al/Si ordering on feldspar dissolution: Part I. Crystallographic control on the stoichiometry of dissolution reaction. *Geochimica et Cosmochimica Acta* 126, 574-594.
- Yuan G., Cao Y., Schulz H., Hao F., Gluyas J., Liu K., Yang T., Wang Y., Xi K., Li F., 2019. A review of feldspar alteration and its geological significance in sedimentary basins: From shallow aquifers to deep hydrocarbon reservoirs. *Earth-Science Reviews* 191, 114-140.
- Zhai Y., 2020. The micro-mechanism of hydrothermal alkaline alteration of K-feldspar and its enlightenment to potash fertilizer production technology, PhD. The University of Chinese Academy of Sciences.
- Zhai Y., Hellmann R., Campos A., Findling N., Mayanna S., Wirth R., Schreiber A., Cabié M., Zeng Q., Liu S., Liu J., 2021. Fertilizer derived from alkaline hydrothermal alteration of K-feldspar: A micrometer to nanometer-scale investigation of K in secondary reaction products and the feldspar interface. *Applied Geochemistry* 126, 104828.
- Zhai Y., Zeng Q., Hellmann R., Liu S., Liu J., Nan J., 2020. Reaction mechanism during hydrothermal alteration of K-feldspar under alkaline conditions and nanostructures of the producted tobermorite. *Acta Petrologica Sinica* 36, 2834-2844.
- Zhang M., Salje E., Carpenter M., Parsons I., Kroll H., Reed S., Graeme-Barber A., 1997. Exsolution and Al-Si disorder in alkali feldspars: Their analysis by infrared spectroscopy. *American Mineralogist* 82, 849-857.
- Zhang X., Wei B., Shang J., Gao K., Pu W., Xu X., Wood C., Sun L., 2018. Alterations of geochemical properties of a tight sandstone reservoir caused by supercritical CO<sub>2</sub>-brine-rock interactions in CO<sub>2</sub>-EOR and geosequestration. *Journal of CO<sub>2</sub> Utilization* 28, 408-418.
- Zhou L., Guo J., Yang N., Li L., 1997. Solid-state nuclear magnetic resonance and infrared spectroscopy of alkali feldspars. *Science in China Series D-Earth Sciences* 40, 159-165.



This work is licensed under a Creative Commons Attribution 4.0 International License CC BY. To view a copy of this license, visit <http://creativecommons.org/licenses/by/4.0/>

